Numerical Study on the Effects of Fuel Injection Characteristics on the Performance of a Lean Burn SG-GDI Engine towards High Efficiency and Emissions Reduction

S. Sarmast[1], M. Ziabasharhagh[1], A. Salavati-Zadeh[2†] and H. R. Fajri[3]

[1] *Mechanical Engineering Faculty, K. N. Toosi University of Technology, Tehran, 19991-43344, Iran*
[2] *Niroo Research Institute (NRI), Tehran, 14686-13113, Iran*
[3] *Iran Khodro Powertrain Co. (IPCO), Tehran, 13988-13711, Iran*

†*Corresponding Author Email: asalavatizadeh@nri.ac.ir*

ABSTRACT

The effects of spark and injection characteristics as well as split injection on the performance and emissions of a spray-guided gasoline direct injection (SG-GDI) engine operating close to stoichiometric conditions are assessed. To accomplish this, a 6-holes injector is simulated and the results are validated against available experimental data for spray penetration length. In addition, an open-cycle multi-dimensional model is developed for a port fuel injection (PFI) engine and the model outcomes are verified against in-cylinder pressure profile and normalized heat release rate. The GDI engine model is yielded under the light of embedment of the above-mentioned models. The model is then employed for investigation of the effects of injector angle, injection pressure, start of first and second injections and two-stage fuel injection with different fuel mass ratios at first and second injections, i.e., split injection, on mixture formation, combustion and engine emissions. The results show the pivotal role of the injector angle on formation of the mixture and output power. On the other hand, it is indicated that while practicing the split injection strategy, the flammability of the relatively stratified lean mixture with fuel to air equivalence ratio of 1.15 around the spark plug, surpasses that of stratified mixture.

NOMENCLATURE

ABDC	After Bottom Dead Center	NO_x	Nitrogen Oxides
ATDC	After Top Dead Center	P	pressure
avg	average	S	standard deviation
BBDC	Before Bottom Dead Center	SA	Spark Advance
BMEP	Brake Mean Effective Pressure	SOI	Start Of Injection
BTDC	Before Top Dead Center	u	relative velocity
CA	Crank Angle	UHC	Unburned Hydrocarbon
CO	carbon monoxide	V	volume
CO_2	carbon dioxide	x_b	the mass fraction burned
d	displacement		
D	droplet diameter	θ	angle (rad)
EVC	Exhaust Valve Closing	λ	air-fuel equivalence ratio
EVO	Exhaust Valve Opening	λ^*	dimensionless wavelength of the most
f	probability density function		unstable waves of liquid-gas interfaces
GIMEP	Gross Indicated Mean Effective Pressure	ρ	density
HRR	Heat Release Rate	σ	gasoline surface tension
inj	injection	φ	fuel-air equivalence ratio
IVC	Intake Valve Closing		
IVO	Intake Valve Opening		

1. INTRODUCTION

Today, internal combustion engines still have a major contribution in power production and human transportation. On the other hand, there is a growing concern regarding the dramatic increase in energy demand, 80% of which is still fulfilled through combustion of fossil fuels. In addition, the environmental impacts of pollutant species generated from combustion of fossil fuels are proved to be responsible for several dangers to human health and mortality. Therefore, the researchers engaged with internal combustion engines have faced the challenge of improvement of combustion efficiency and lowering the emissions to meet the rapid responses required by regulatory agenda.

The quality of the air-fuel mixture, which is highly dependent on characteristics of fuel injection, is pivotal to achieve high combustion efficiency. In this framework, enhancing the precision in controlling the injection process is of crucial importance. This has paved the way through development of numerous injection strategies, e.g., port fuel injection. Gasoline direct injection is regarded as a promising initiative strategy compared with PFI. This injection scheme deals with spraying the fuel directly into the combustion chamber and gives much more precision in controlling the amount of fuel along with injection timing and duration. Meanwhile, the lower temperature and pumping losses resulting from direct injection, makes GDI engines surpass PFI ones in volumetric and thermal efficiency along with compression ratio, and provides them better performance in cold start and transient response during load variations (Chen *et al.,* 2017). These advantages have made this technology be attractive for scientists and engineers, and many researches have also addressed embedment of GDI with other technologies, e.g. using fuel blends (Wang *et al.,* 2015) and EGR (Lattimore *et al.,* 2016).

There are two combustion modes in GDI engines with respect to injection timing: the homogeneous charge, i.e., early single injection at high engine loads and speeds, and stratified charge which corresponds to late single or double injection at idle, low and medium engine loads and speeds (Costa *et al.,* 2012; Drake *et al.,* 2007; Alkidas *et al.,* 2003). For stratified charge, there are three approaches depending on the relative position of the injector and the way that fuel is guided to the spark plug; In wall guided strategy, the injector is side mounted and fuel is guided by the bowl shaped piston (Xu *et al.,* 2009; Yi *et al.,* 2009; da Costa *et al,* 2015; Catapano *et al.,* 2016 a), unlike air guided approach in which the fuel injected from the side-mounted injector is guided by the airflow (da Costa *et al.,* 2015; Catapano *et al.,* 2016 b; Cathcart *et al.,* 2000). On the other hand, the spray guided direct injection spark ignition (SG-DISI) strategy, in which the injector is placed nearby the spark plug (Vanderwege *et al.,* 2003; Wang *et al.,* 2014), is proved to have the potential to increase fuel economy especially under a stratified charge mode (Vanderwege *et al.,* 2003; Szekely *et al.,* 2005; Park *et al.,* 2012).

Despite the fact that experimental observations, especially those employing optical accessible engines (Catapano *et al.,* 2016(a); Wang *et al.,* 2017(a); Costa *et al.,* 2016; Marseglia *et al.,* 2017; Merola *et al.,* 2016) are proved to be useful tools in overcoming challenges regarding combustion development of the engines utilizing GDI strategy, the critical role of numerical simulation in obtaining rapid responses with feasible costs have made researches to employ computational fluid dynamics (Boccardi *et al.,* 2016; Zheng *et al.,* 2015; Banerjee *et al.,* 2016; zhao An *et al.,* 2016) in the processes of design and optimization.

Most of the studies regarding the GDI engines are two-fold. One of the aspects brings the spray-wall interaction into account (Schulz *et al.,* 2014; Montanaro *et al.,* 2012; Catapano *et al.,* 2016 b). It has been indicated that the impingement of liquid fuel on the combustion chamber wall and piston is a possible source for unburned hydrocarbon (UHC) and particulate matter emissions (Bonatesta *et al.,* 2014; Wang *et al.,* 2016). This impingement is usually modelled under the light of employing the mundo-sommerfeld and kuhnke models (Montanaro *et al.,* 2016; Moreira *et al.,* 2011; Kuhnke, 2004).

Analyzing and optimizing the formation of air-fuel mixture is another important issue that has been brought under study by many researchers (Costa *et al.,* 2012; Boccardi *et al,* 2016; Bonatesta *et al.,* 2014; Iyer *et al.,* 2009; Dempsey *et al.,* 2012). It is shown that in GDI engines, the mixture formation in the combustion chamber depends strongly on the fuel injection parameters such as injector angle and start of injection (SOI hereafter), the shape of the piston and swirl and tumble ratios. Since imperfect mixing and wall wetting results in formation of UHC and soot, the intake ports and combustion chamber should be designed to achieve a moderate or high tumble ratio (Rivera *et al.,* 2010). In addition, the ignition timing and start of injection influence the combustion process (Hallgren *et al.,* 2003; Kaiser *et al.,* 1999). Hence, optimizations of SOI, injection pressure, injection duration and injection direction are very important and effective on output power and emissions.

Taking the crucial role of the above mentioned injection characteristics into account, the present research aims to explore the effects of injection parameters on the combustion characteristics of a SG-DISI engine. In this framework, the analysis is accomplished in 5 aspects as follows:

1- The effect of Injector angle;

2- The effect of SOI for the first and second injections;

3- The effect of injection pressure;

4- The effect of ignition timing;

5- The effect of different split injection strategies;

To this end, in the first step, a high pressure spray with six asymmetric jets is simulated using AVL Fire v. 2014 software (AVL Fire user's guide). The case study is a constant volume chamber containing

nitrogen gas, and three different injection pressures are investigated. A comprehensive one-dimensional model is then utilized to model a four-stroke PFI 1649 cc engine at full and part load operating conditions. The 3-dimensional CFD simulations are carried out in the next step using the calibrated results obtained from the thermodynamic model. AVL Fire v. 2014 is employed and the validation of the results is carried out against the experimental observations in IPCO for the same engine. The model is then used for investigating the effects of injection pressure, start of first and second injection as well as the effects of split injection on the mixture formation, combustion and engine emissions. In addition, appropriate angle for optimization of mixture formation is obtained. Finally, the fuel consumption, emissions and output power of EF7 engine are compared for port direct injection strategies.

As mentioned, to develop the GDI engine model the following steps should be accomplished:

1) Simulation of an injector and validation of the results against experimental observations.

2) Thermodynamic cycle simulation and model calibration of the baseline PFI engine.

3) Utilizing the results of the thermodynamic model as boundary conditions for 3D simulation of the baseline PFI engine and validation of the results against experimental data.

4) Embedment of the models obtained through steps 1 and 3 to investigate the performance of the GDI engine.

2. GDI INJECTOR MODEL

2.1 Experimental Setup and Data

To find the appropriate values to be employed in simulation of the injection, a 6-hole bosch HDEV 5.1 with 0.193 mm inner diameter is selected. The numerical simulation results are validated against the experimental findings reported by istituto motori-CNR for two different amounts of injected fuels at three different injection pressures (Costa *et al.,* 2011). The amount of fuel injected and the injection pressure for each case is brought in Table 1. The fuel was injected in a constant volume chamber optically accessible that contains nitrogen gas at the pressure of 0.1 MPa and the temperature of 298 K. The schematic of the experimental setup and the spray footprint on a plane placed at 30 mm from the nozzle holes is depicted in Fig. 1. Table 1 also elucidates the values of validation coefficients for different injection pressures (C_1).

Table 1 Cases studied for spray simulation validation

Case	Pressure, MPa	C_1	Fuel Mass Injected , mg
1	20	6	50
2	10	4	50
3	6	4	10

2.2 Spray Simulation Methodology and Results

In the spray simulation, both eulerian and lagrangian approaches are widely used. Since in the area closer to the nozzle outlet spray is much denser, lagrangian approach is not appropriate for this area. On the other hand, spray simulation by eulerian approach is not recommended in areas further from the nozzle where the spray becomes dilute. So, the eulerian-lagrangian approach is an ideal way for spray simulation. This approach requires a fine mesh near the nozzle that has interface with the main domain, i.e., the combustion chamber (Wang *et al.,* 2017 b).

In the present research, a more common approach, discrete droplet model (DDM), is employed. This methodology uses eulerian and lagrangian formulations for gas phase and discrete droplets, respectively. The spray primary breakup is modeled considering probability density distribution functions around a mean diameter. The mean diameter D_{mn} can be calculated from Eq. (1) (Sirignano, 1999). Where, D is droplet diameter, $f(D)$ is the probability density function and m and n are constants. In the present research, the log-normal distribution function is used to estimate the initial size of the droplets, in which, the mean diameter and standard deviation should be known. Semi-empirical Eq. (2) is used to find the average diameter (D_{avg}). Also, Eqs. (3) and (4) show the standard deviation (s) in terms of injection pressure (P_{inj}) and log-normal distribution function, respectively (Costa *et al.,* 2011).

$$D_{mn} = \frac{\int_0^\infty f(D)D^m dD}{\int_0^\infty f(D)D^n dD} \tag{1}$$

$$D_{avg} = C\frac{2\pi\sigma\lambda^*}{\rho_g u_{rel}^2} \tag{2}$$

$$s = 0.1\left(0.1P_{inj} - 1\right) + 0.5 \tag{3}$$

$$f(D) = \frac{1}{D\sqrt{2\pi}s}\exp\left(-\frac{(\log D - \log D_{avg})^2}{2s^2}\right) \tag{4}$$

Where, σ, λ^*, ρ_g and u_{rel} are the gasoline surface tension, the dimensionless wavelength of the most unstable waves of liquid-gas interfaces, the gas density and relative velocity between fuel jet and surrounding gas, respectively. The parameter C is considered to be equal to 1. The huh-gosman sub-model, a turbulence-induced atomization model is appropriate for GDI multi-hole injector (Costa *et al.,* 2011), is employed for simulating secondary breakup. In addition, the evaporation is simulated using dukowicz evaporation model, which is commonly used for GDI spray (Costa *et al.,* 2011).

Basis of this model is analogy between heat and mass transfer processes in the vicinity of the droplet. The collision of the droplets is simulated utilizing nordin model (Taskiran *et al.,* 2014) which has the major
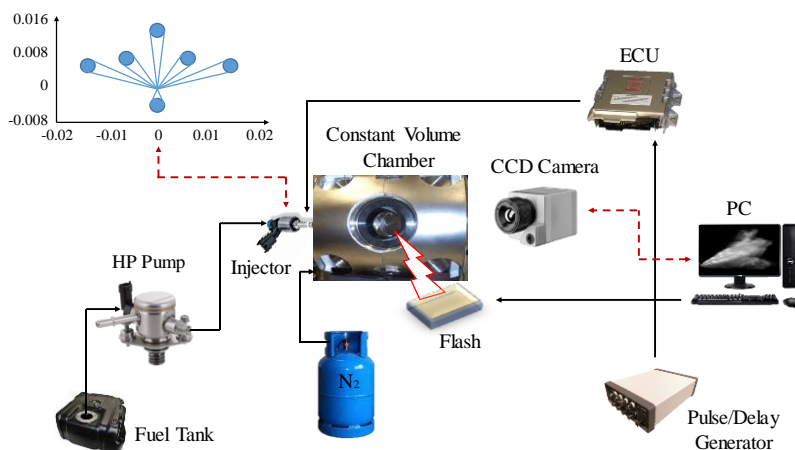
Fig. 1. Experimental setup for spray imaging (Costa *et al.* 2011).

advantage of mesh size independency over the conventional o'rourke and amsden model (Semenov *et al.,* 2013). In this method, by knowing the position and velocity of every particle, the minimum distance between two particles and the time required for impact will be obtained. The probability of collision is then determined and a random number between zero and one is chosen. If the random number is less than probability, it is assumed that the collision is accomplished.

xIn the present research, AVL Fire software is used for spray simulations utilizing $k - \varepsilon$ turbulence model and simple algorithm for pressure-velocity coupling. The convergence limits for momentum, kinetic energy and dissipation rate are 1e-06. Figures 2, 3 and 4 show the tip penetration, relative pressure and spray images, respectively. In determining the tip penetration, three factors always play the key role: droplets size, injection pressure and fluid resistance, i.e., drag force. Increasing the drag force reduces the penetration length, whereas increasing the size of the droplets has the opposite influence. As seen in Fig. 3, the drag forces at the injection pressure of 20 MPa are higher than the other two modes. Also, the droplets diameters are smaller at the injection pressure of 20 MPa due to better fuel atomization. As a result, it is expected that the penetration length should be less at the injection pressure of 20 MPa. Nevertheless, the results indicate that with increasing injection pressure the penetration length increases. This proves that increasing injection pressure is very effective in determining the penetration length and also dominates the other factors.

3. MODELING THE BASE PFI ENGINE

The EF7 MPFI CVVT engine with 1649 cc volume is studied at two operating condition (full and part loads).

For 3D simulation of combustion, the initial conditions of combustion chamber at the start of simulation (intake valve opening) are found via experimental observations in IPCO. Nevertheless, to find appropriate inlet-outlet boundary conditions, a comprehensive 1D engine model is developed using

the GT-Power software. The calibrated instantaneous mass flow rate is used as boundary conditions for inlet port and the average static pressure is used as boundary condition at exhaust port. The 3D simulations are carried out using AVL Fire software from the intake valve opening (IVO) to the exhaust valve opening (EVO). This includes 549 degree of crank angle, about 90 degree of which both valves are open. The engine details, test parameters relevant to the operating conditions and exhaust gas analysis are presented in Tables 2, 3 and 4, respectively.
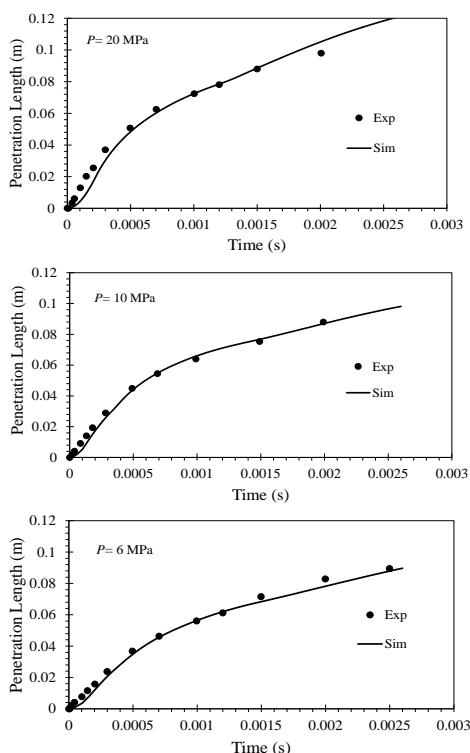

Fig. 2. Tip penetration of spray in different injection pressure.

3.1 One Dimensional Gas Dynamic Model

Figure 5 shows the schematic of the one dimensional

MPFI EF7 engine model. The gas is assumed to be ideal and the wiebe function (Eq. (5) (Ghojel, 2010)) is used to represent the flame propagation.

$$x_b = 1 - \exp\left[-a\left(\frac{\theta - \theta_0}{\Delta \theta}\right)^{m+1}\right] \tag{5}$$

Where, m and a are calibration factors, and θ_0 is the crank angle corresponding to the start of combustion. In the present model, the calibrated values are found to be 1.53 for m, and 2.31 for a. The zeldovich mechanism for formation of NOx and woschni's equations for in-cylinder heat transfer are considered.
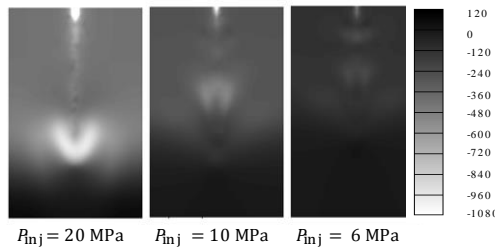
$P_{inj} = 20$ MPa $P_{inj} = 10$ MPa $P_{inj} = 6$ MPa
Fig. 3. Relative pressure (Pa).
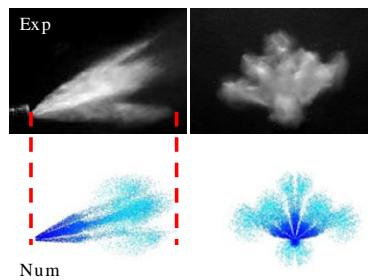
Fig. 4. Spray images for injection pressure of 20 MPa.
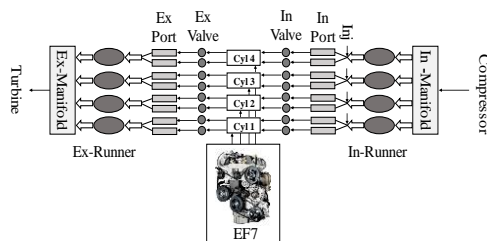
Fig. 5. Schematic of 1D simulation of EF7 engine.

In order to assure the correctness of the one dimensional model, the in-cylinder pressure profiles obtained from numerical simulation and experiment at full and part loads are illustrated in Fig. 6. An assessment on the results will prove the correct calibration of the flow and in-cylinder parameters as the compression and combustion processes are well reconstructed. In addition, the mass flow rate obtained from one dimensional model which is used as boundary condition at intake port for 3D model is depicted in Fig. 7.

3.2 Three Dimensional CFD Modeling of PFI Engine

The computational grid of EF7 engine at IVO, along with the location of spark plug and injector for PFI

and GDI conditions are illustrated in Fig. 8. Extended coherent flame model with 3 zones containing air+EGR, fuel and mixing zones (ECFM-3z hereafter) model is employed for combustion simulation. Simulating combustion in this framework is carried out under the light of employing a stretch factor to account for burning velocity and an initial flame surface density to bring ignition delay under consideration. The equilibrium reactions embedded with ECFM-3z model are brought in Eqs. (6a) to (6j) (Colin *et al.,* 2004).
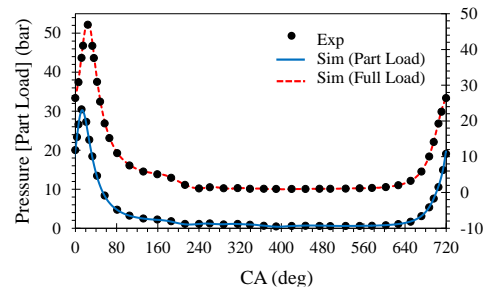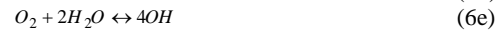
$$N_2 \leftrightarrow 2N \tag{6a}$$
$$O_2 \leftrightarrow 2O \tag{6b}$$
$$H_2 \leftrightarrow 2H \tag{6c}$$
$$O_2 + H_2 \leftrightarrow 2OH \tag{6d}$$
$$O_2 + 2H_2O \leftrightarrow 4OH \tag{6e}$$
$$O_2 + 2CO \leftrightarrow 2CO_2 \tag{6f}$$
$$CO + OH \leftrightarrow CO_2 + H \tag{6g}$$
$$O_2 + N_2 \leftrightarrow N + NO \tag{6h}$$
$$O_2 + N \leftrightarrow O + NO \tag{6i}$$
$$N + OH \leftrightarrow H + NO \tag{6j}$$

Fig. 6. Experimental and numerical results for in-cylinder pressure profile for full and part load conditions.
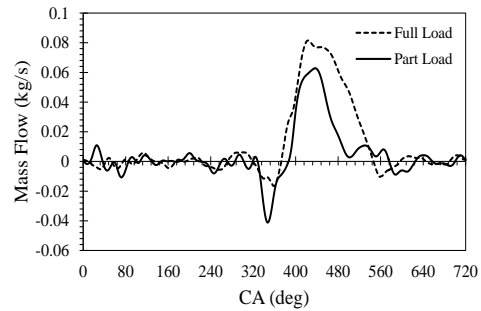

Fig. 7. Mass flow rate variations as boundary condition at inlet of intake port.

The in-cylinder flow is simulated using the continuity, momentum, energy, viscous heating and pressure work equations, k-zeta-f turbulence model and metghalchi and keck correlation for laminar flame speed Simple/Piso algorithm is utilized for pressure-velocity coupling. The convergence limits for all key parameters are 1e-06.

4. SIMULATION RESULTS FOR BASE PFI ENGINE

4.1 Grid Study

Three different grids are created for mesh study

(Table 5). Figure 9 illustrates the comparison of in-cylinder pressure for different sizes of grid cells at full load condition. An assessment of the results indicates an almost negligible discrepancy between the results obtained from the first two cases, i.e., 800,000 and 1,300,000 grids. In spite of this, utilizing 800,000 meshes will cause oscillation in the value of residuals in some time steps. Therefore, the case with 1,300,000 grids is used.

Table 2 Engine details

xEngine (EF7)	4 stroke spark ignition 4 in line cylinders 4 valves per cylinder MPFI, CVVT and TWC
Displacement	1649 cc
Stroke	85 mm
Bore	78.6 mm
Compression ratio	11
Max power	82 kW @ 5750 rpm
Max torque	150 Nm @ 3300rpm
Fuel	Gasoline (Octane 95)

Table 3 Test parameters

Engine speed	3000 rpm	
Parameters	Part Load	Full load
BMEP (bar)	4.015	11.045
IVO	57° BTDC	54° BTDC
IVC	38° ABDC	41° ABDC
EVO	45° BBDC	45° BBDC
EVC	32° ATDC	32° ATDC
SA	33.85°	13.85°
Fuel consumption (kg/h)	4.899	12.37
Lambda	0.999	0.901
Initial temperature (K)	1000	1100
Initial pressure (bar)	1.0645	1.2215

Table 4 Exhaust gas analysis

Engine speed	3000 rpm	
Component	Part Load	Full load
CO (vol%)	0.64%	3.47%
CO_2 (vol%)	14.71%	12.68%
HC (ppm)	943.1	1172.8
NOx (ppm)	2003.67	975.73
O_2 (vol%)	0.4%	0.07%

Table 5 Specification of used meshes

Grid NO.	Number of cells	Simulation time (h)	Max in-cylinder pressure (bar)
1	~1300000	44	47.87
2	~800000	36	48.86
3	~550000	31	45.75

4.2 Results Validation

The numerical simulation results and experimental findings for pressure and heat release rate in full and part load conditions are depicted in Fig. 10 which is

in very good consistency. The deviation between the pressures during the compression stroke does not exceed 3%, which proves the acceptable accuracy also in prediction of the amount of mass trapped.

In addition, the simulation results for velocity magnitude in a plane through the valves during exhaust and intake are depicted in Fig. 11. The propagation of flame front at full load condition is illustrated in Fig. 12.
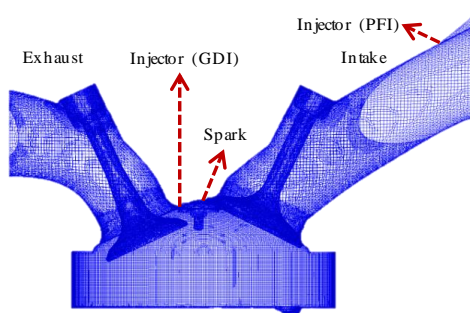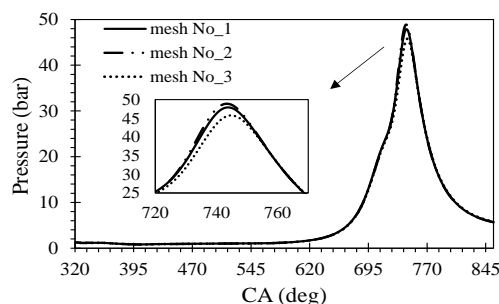

Fig. 8. Computational grid of EF7 engine at IVO.

Fig. 9. Comparison of in-cylinder pressure by changing the size of grid cells at full load condition.
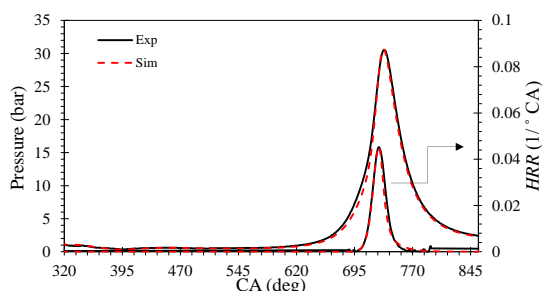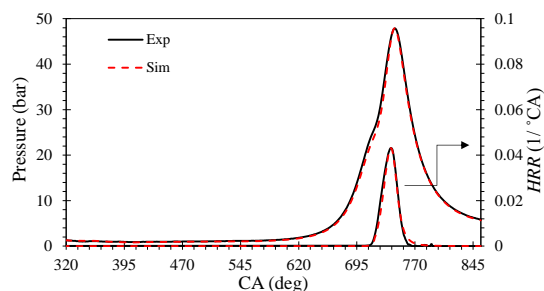

Fig. 10. Comparison of simulated and experimental results of pressure and heat release rate for full load (top) and part load (bottom).
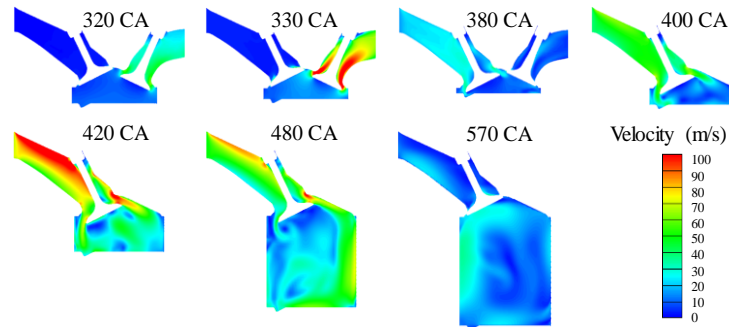
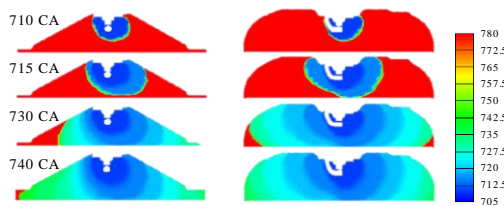**Fig. 11. Velocity magnitude through intake (left) and exhaust (right) valves, Firing TDC is 720°CA.**

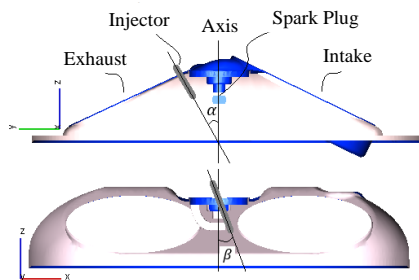**Fig. 12. Flame front propagation in the combustion chamber at full load.**

Fig. 13. Injector location on engine cylinder head.

5. GDI ENGINE SIMULATION RESULTS

In the presented results, it is aimed to investigate the effects of the following parameters on the engine performance characteristics:

1) Injector angle;

2) The first and second fuel injection timings;

3) Injection pressure;

4) Ignition timing;

5) Split injection strategy.

5.1 Effect of Injector Angle

It seems pivotal to determine the injector angle and orientation of fuel spray jets. This orientation of the jet is characterized by two angles, i.e., α and β, as illustrated in Fig. 13. The effects of changing these angles on the indicated mean effective pressure is brought in Fig. 14.

The fuel injection is set to be started at 450° CA under the pressure of 6 MPa and end at 475° CA. According to Fig. 14, it could be indicated that $\alpha = 40$ is an appropriate angle for corresponding to the maximum output power. In order to determine the

optimum β, the fuel is considered to be injected at angles 0, 10, 20 and 30 relative to the cylinder axis with constant $\alpha = 40$. The results show that $\beta = 10$ is the best injector angle in x-z plane. The simulations are then repeated for $\beta = 8.5$ and $\beta = 11.5$. Based on the results, $\beta = 10$ still ends in the optimum engine performance relative to its adjacent angles.
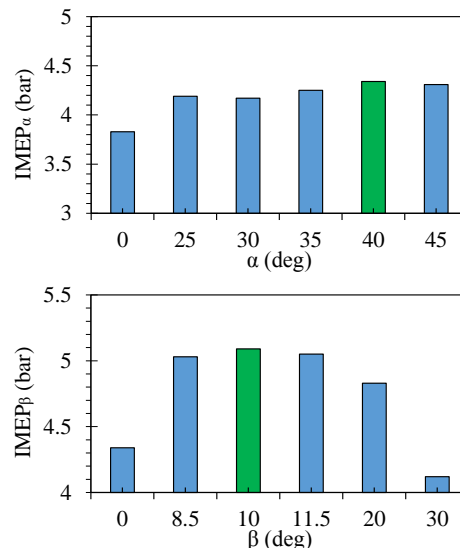

Fig. 14. Effects of angle α and β on indicated mean effective pressure (P_{inj}=6MPa, SOI=450° CA.)

The impact of injector angle on the performance of the engine can be justified by exploring the effect of injector angles, α and β, on distribution of fuel-air equivalence ratio (φ) in the cylinder. Therefore, the contours for φ at the time of ignition versus different α and β are depicted in 2 different perpendicular vertical planes in Figs. 15 and 16, respectively. It could be indicated from the results that the most homogeneous distribution of φ is yielded for $\alpha = 40$ and $\beta = 10$.

5.2 Effect of Timing for the Case of Single Injection

In the next step, the influence of SOI on the burning characteristics is brought under study. To accomplish this, the numerical simulations are carried out for three injection pressures of 6, 10 and 20 MPa with SOI changing from 430° CA to 530° CA. Also, when using single injection strategy, long delay in fuel

injection prevents the formation of suitable mixture at ignition timing. Figure 17 shows the effect of SOI as well as injection pressure on indicated mean effective pressure and mean reaction progress variable. According to the simulation results, SOI 450° CA in all three injection pressures causes the maximum output power in single injection conditions.
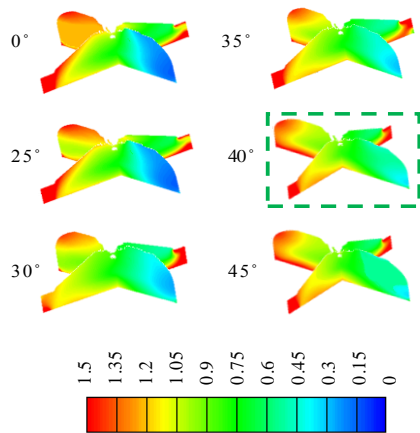

Fig. 15. Equivalence ratio in planes going through the spark plug at ignition timing for different angles of *α*.
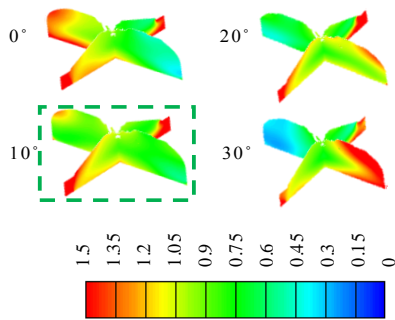

Fig. 16. Equivalence ratio in planes going through the spark plug at ignition timing for different angles of *β*.

5.3 Effect of Injection Pressure on Combustion Performance

Figure 18 shows the in-cylinder pressure profile at different injection pressures. In addition, the *φ* in planes going through the spark plug at the ignition timing is illustrated in the same figure. From Fig. 18 it could be indicated that the injection pressure of 10 MPa ends in the most uniform distribution of *φ* along with the highest amount of IMEP.

The effects of injection pressure on the performance of GDI engines are two-fold. When the injection pressure is lowered, despite weak atomization and evaporation of the fuel jet, a longer mixing time will be provided for fuel and air streams. This makes injection pressure have key influences when injection is delayed, which is addressed by many researchers, e.g., (Costa *et al.,* 2016). On the other hand, for case of early injection, as could be indicated from Fig. 18, injection pressure does not

have a significant impact on output power in GDI engines. Additionally, the flame front propagation in GDI engine with injection pressure of 10 MPa is depicted in Fig. 19.
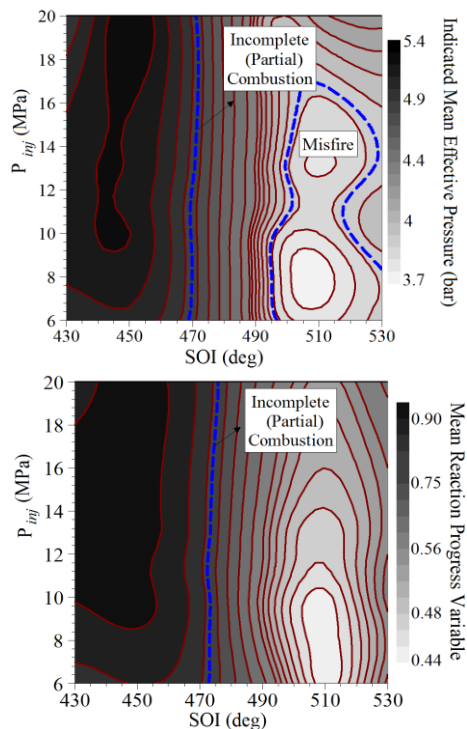

Fig. 17. Comparison of combustion characteristics at different start of injection and injection pressures.
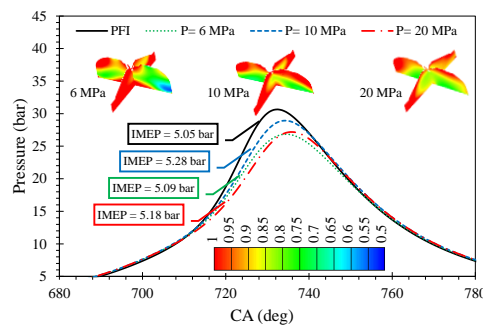

Fig. 18. Effect of injection pressure on in-cylinder pressure.

5.4 The Effect of Ignition Timing on Combustion Performance

In GDI engines, due to more air entrance into the combustion chamber resulting in higher air-fuel equivalence ratio ($λ = 1.04$ in this research) and lower temperature, the output power can be increased by spark advance, which may lead to knocking because of the possibility of auto-ignition of unburned mixture. This proves the significance of determination of ignition timing. For this purpose, the empirical knock model, which is based on an empirical approach identifying the possibility of knock occurrence within specified regions depending on different parameters, is utilized. The most influential parameters on the knock probability

are detected to be the amount of EGR, the temperature, the progress variable and the mixture mass fraction, respectively (Esfahanian *et al.,* 2014).

Table 6 shows the ignition timings for four simulated cases. Spark advance more than 39.85° CA leads to auto-ignition which may end in heavy knock and damage. For comparison of output power of simulated cases, gross indicated mean effective pressure (gIMEP) is calculated from Eq. (7), where V_d is displacement volume, P and V are in-cylinder instantaneous pressure and volume, respectively.

$$(gIMEP)_{closevalve} = \frac{1}{V_d} \int_{IVC}^{EVO} p dV \qquad (7)$$

Table 7 shows the results of emissions and output power for four different ignition timing of GDI engine compared with the PFI mode. According to the results, the GDI engine performance surpasses the PFI engine in all simulated cases. In the cases of GDI 2 and GDI 3, nitrogen oxides (NO_x) are reduced by 45.3% and 29%, CO is reduced 27.8% and 27.95%, CO_2 is reduced 6% in spite of 4.32% and 4.82% increase in gIMEP, respectively.

5.5 Effect of Start of Second Injection

Two or multi-stage fuel injection causes better air-fuel mixture formation in combustion chamber in direct injection engines. Under these conditions, for early primary or secondary injection, there is sufficient time for evaporation of fuel and a relatively homogeneous mixture is formed in the chamber. In late injection, rich mixture is usually formed around the spark plug.

In general, it is indicated that with increase in the engine load, the use of early injection is recommended to form a homogeneous mixture and achieve higher output power. In lower engine loads or idle conditions, late injection is used for formation of a rich mixture around the spark plug and lean mixture farther to reduce fuel consumption. The present research aims to explore the effect of start of second injection as well as split injection for part load condition. To this end, the injection pressure of 10 MPa, the start of first injection of 450° CA, the best condition for single injection according to presented results, are opted. 70% of fuel is sprayed in the first stage and the remaining (30%) is injected in the second stage. Figure 20 shows the in-cylinder pressure for different times of start of second injection.

The effects of start of second injection on fuel-air equivalence ratio near the spark plug and in planes passing through the spark plug at the time of ignition along with the NOx emission at exhaust valve opening are illustrated in Fig. 21.
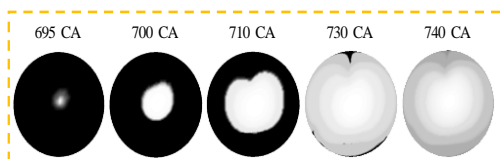
According to Fig. 21, in very late secondary injection (620° CA to 640° CA (red box)), the mixture with the φ above 1.6 is formed around the spark plug. The simulation results show that for the two-stage injection, relatively homogeneous lean mixture (green box) results in better combustion characteristics at part load condition compared to the stratified mixture (red and orange boxes). Also, in 580° CA to 620° CA (orange rectangle), the air-fuel mixture is rich near the exhaust valves that may lead to knocking. Therefore, according to the simulation results when the start of second injection is 500° CA more complete combustion is performed due to the formation of homogeneous mixture with equivalence ratio 1.15 around the spark plug.

Table 6 Different spark advances (SA)

Case	Ignition Timing (°CA)	Spark Advance (°CA)
GDI 1	690.15	29.85
GDI 2	686.15	33.85
GDI 3	683.15	36.85
GDI 4	680.15	39.85

Table 7 Comparison of engine operating parameters for different spark advances (SA)

Parameter	PFI	GDI 1	GDI 2	GDI 3	GDI 4
NOx (PPM)	2000	626	1094	1420	1820
CO (%)	0.59	0.48	0.431	0.430	0.51
CO2 (%)	12.59	11.69	11.75	11.76	11.83
gIMEP (bar)	5.055	5.18	5.28	5.31	5.26

5.6 Effect of Split Injection

To suppress the negative impacts of increase in turbulent kinetic energy on mixture flammability and combustion stability, the strategy of split injection is employed in GDI engines, i.e., the fuel is injected in two different stages.

In this paper, split injection strategy is utilized to show the significant role of injected fuel mass ratios on engine performance and emissions. Since the injected fuel mass ratio has great influence on φ near the spark plug in double injection, the effects of split injection on the equivalence ratio especially near the spark plug at the ignition timing, in-cylinder pressure and the amount of nitrogen oxides are studied.
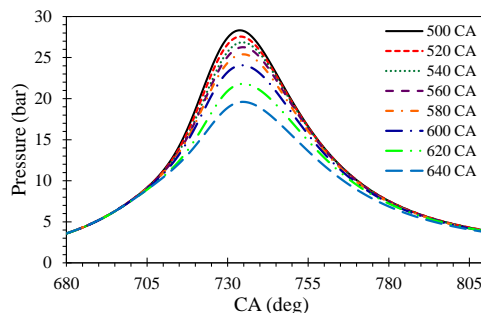

Fig. 20. Effect of start of second injection on in-cylinder pressure (P_{inj}=10 MPa, SOI$_1$=450 CA, injected fuel mass ratio=7:3).

Fig. 19. Flame front propagation of GDI engine.

S. Sarmast *et al.* / *JAFM*, Vol. 12, No. 3, pp. 763-776, 2019.
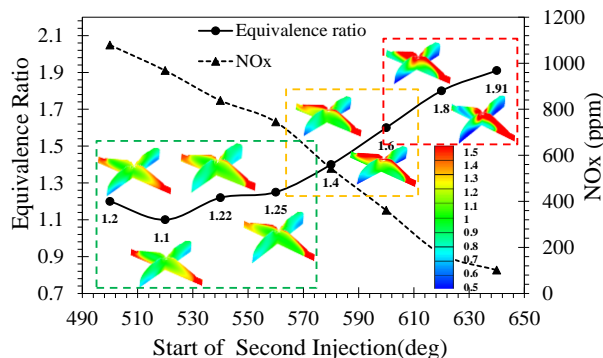
Archive of SID

Fig. 21. Effects of start of second injection on fuel-air equivalence ratio near the spark plug and in planes passing through the spark plug at the time of ignition and NOx emission at EVO (P_inj=10 MPa, SOI_1=450 CA, injected fuel mass ratio=7:3).

To accomplish this, the first and second injections are done at angles of 450° CA and 500° CA, respectively. The mass ratio of primary to secondary injection has been changed from 0%-100% to 100%-0% (the first percentage represents the ratio of first stage of injection at 450° CA and the second percentage indicates the ratio of second stage of injection at 500° CA). Figure 22 shows the effect of split injection on (a) the fuel-air equivalence ratio near the spark plug at the time of ignition and NOx emission at exhaust valve opening, (b) λ and (c) φ in planes going through the spark plug. Figure 23 shows the effect of split injection on in-cylinder pressure for investigated cases.

According to the results of Fig. 22, in ratios of 80%-20% and 90%-10% more homogeneous air-fuel mixture is formed, while in the ratio of 10%-90% and 20%-80%, one side of the chamber is much leaner than the other side. According to Fig. 23, the ratios of 80%-20% can produce more power than other ratios, but this increase is very small compared to single injection with more nitrogen oxides formed. Table 8 shows the performance and emissions of EF7 engine in PFI and GDI with single or double injection in studied cases.

According to the results presented in Table 8, as the amount of the fuel injected at the second stage increases, more complete combustion is yielded causing higher indicated mean effective pressure and higher rate of conversion of fuel to carbon dioxide, ending in lower carbon monoxide. Moreover, higher temperature in the reaction zone causes more NOx to be present in cylinder emissions.

In addition, the effect of split injection on tumble ratio is assessed for various conditions. According to Fig. 24, the tumble ratio in ratios of 80%-20% and 90%-10% is higher than the case of single injection (100% at 450° CA). This results in better mixing of air-fuel mixture and increasing the output power of the engine, considering the expected shorter time required for formation of flame kernel. Figure 25 shows the mean reaction progress variable for the cases brought in Fig. 24. As it can be seen in Fig. 25, the rate of fuel burning in the start of combustion in the ratios of 50%-50% to 90%-10% is more than single injection because the fuel-air equivalence ratio around the spark is higher than unity (according to

Fig. 22(a)). Finally, in the ratios of 80%-20% and 90%-10% more complete combustion is occurred due to the relatively homogeneous lean mixture.
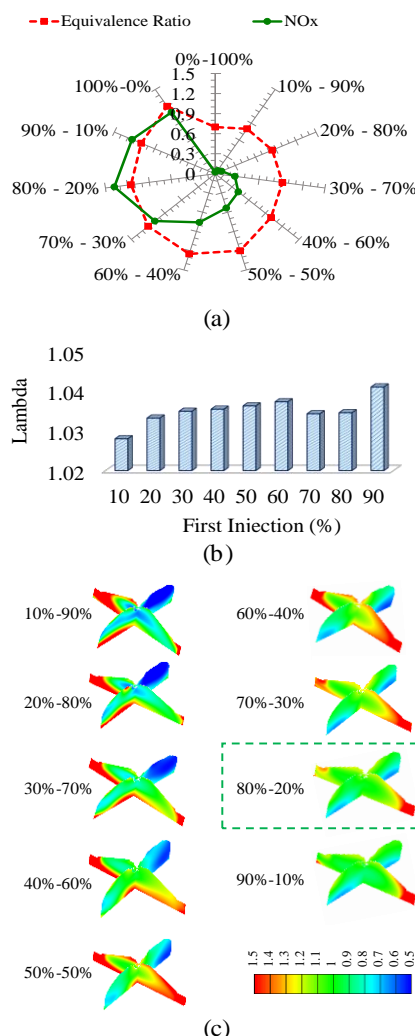

(a)

(b)

(c)

Fig. 22. Effect of split injection on (a) the fuel-air equivalence ratio near the spark plug at ignition timing and NOx emission (ppm) at EVO, (b) in-cylinder air-fuel ratio and (c) the fuel-air equivalence ratio in planes that through the spark plug (P_inj=10 MPa, SOI_1=450 CA, SOI_2=500 CA).

Table 8 Comparison of performance and emissions formation for different split injection

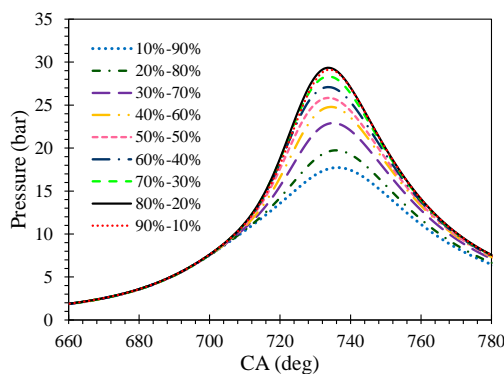| Parameter	0%-100%	10%-90%	20%-80%	30%-70%	40%-60%
NOx (PPM)	31	57	94	346	415
CO (%)	2.73	2.57	2.37	1.53	1.38
CO_2 (%)	5.23	8.31	8.94	9.73	10.65
gIMEP (bar)	3.27	3.85	4.06	4.46	4.56
50%-50%	60%-40%	70%-30%	80%-20%	90%-10%	100%-0%
541	757	1079	1380	1380	1095
1.2	0.99	0.72	0.48	0.43	0.43
10.91	11.1	11.5	11.8	11.8	11.7
4.53	4.89	5.15	5.32	5.30	5.28

Fig. 23. Effect of split injection on in-cylinder pressure (P_{inj}=10 MPa, SOI$_1$=450 CA, SOI$_2$=500 CA).
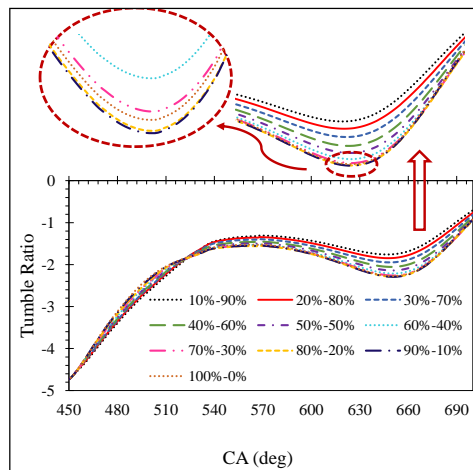

Fig. 24. Effect of split injection on tumble ratio (P_{inj}=10 MPa, SOI$_1$=450 CA, SOI$_2$=500 CA).

6. CONCLUSIONS

The present research aims to study the effects of spark and injection characteristics as well as split injection on the performance and emissions of a spray guided gasoline direct injection (SG-GDI) engine and to compare it with port fuel injection engine.
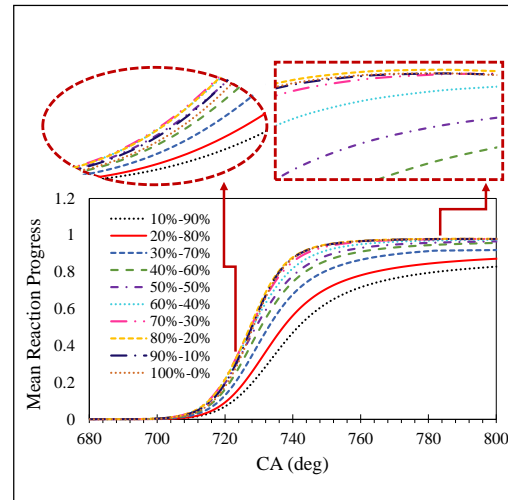

Fig. 25. Effect of split injection on mean reaction progress (P_{inj}=10 MPa, SOI$_1$=450 CA, SOI$_2$=500 CA).

To accomplish this, a high pressure spray with six asymmetric jets is simulated in a constant volume chamber containing nitrogen gas in three different injection pressures. The results are validated against the experimental observations reported by istituto motori-CNR. To simulate the combustion, the four stroke EF7 engine with 1649 cc is simulated at full and part load conditions using 1D (gas dynamics) and 3D (an open-cycle model) approaches. These models outcomes are verified against in-cylinder pressure profile and normalized heat release rate. The model is then embedded with the injector models to yield the final GDI engine model. The model is then employed to study the effects of injector angle, start of injection, ignition timing as well as split injection on the performance of engine toward high efficiency and emissions reductions. In the following, the most significant results are mentioned.

- The droplets sizes, injection pressure and fluid resistance (drag force) have essential roles in determining the spray penetration length simultaneously. The results prove that at higher injection pressure, the droplets diameter is smaller compared to the low injection pressure due to the better fuel atomization. Reduction in the droplets sizes lowers the penetration length. Also, the drag forces increase monotonically by increasing the injection pressure. Therefore, it is expected that the penetration length is lower at high injection pressure. The results show that with increasing injection pressure, the spray penetration length increases. This properly shows that injection pressure is very effective in determining the penetration length and dominates the other factors.

- The simulated results of single injection cases showed that the injector angle is extremely effective on the mixture formation and output power. In this study, the angles of $\alpha = 40$ and $\beta = 10$ (according to the Fig. 13) are found to be appropriate angles for developing homogeneous mixture and maximizing the output power.

- The results indicate that for the engine operating conditions opted for the present study, in which the injection is accomplished during the intake stroke, the injection pressure is not very effective on the results. This result is consistent with outcomes of other researches (Costa *et al.,* 2016), in which the injection pressure was found to be influential in case of late injection.

- The results prove the optimum time for start of single injection to be 450° CA in all three injection pressure. At this time, a relatively homogeneous mixture, relatively rich around the spark plug ($_\varphi$) and slightly lean in farther areas, is formed. At injection pressure of 10 MPa, the GDI 2 and GDI 3 cases (according to the values in Table 8 and based on different ignition timings) nitrogen oxides (NOx) are reduced by 45.3% and 29%, CO is reduced by 27.8% and 27.95%, CO_2 is reduced by 6% and gIMEP is increased by 4.32% and 4.82%, respectively. According to these results, all GDI simulated cases have better performance compared to PFI engine.

- When using double injection strategy, a long delay in secondary injection (injection in compression stroke) causes forming a rich mixture around the spark plug. Meanwhile based on the results, the flammability of relatively homogeneous lean mixture with the fuel to air equivalence ratio of 1.15 around the spark plug is more compared to the stratified mixture. Also, using the split injection, the mixture equivalence ratio is more controllable at the time of ignition. In the split injection with ratios of 80%-20% and 90%-10%, nitrogen oxides (NOx) are reduced by 31% and 38%, CO is reduced by 19% and 28%, CO_2 is reduced by 6.4% and gIMEP is increased by 5.24% and 4.53% comparing to PFI engine, respectively. Therefore, despite more reduction of pollutants when using single injection strategy, double injection results in more increase of output power. In addition, the volumetric efficiency is 4.5% higher than the PFI engine.

ACKNOWLEDGEMENTS

REFERENCES

Alkidas, A. C. and S. H. E. Tahry (2003). Contributors to the fuel economy advantage of DISI engines over PFI engines. *SAE Technical Paper* 2003(01), 3101.

AVL FIRE User guide, version 2014, AVL List GmbH, 2015.

Banerjee, R. and S. Kumar (2016). Numerical investigation of stratified air/fuel preparation in a GDI engine. *Applied Thermal Engineering* 104, 414-428.

Boccardi, S., F. Catapano, M. Costa, P. Sementa, U. Sorge and B. Vaglieco (2016). Optimization of a GDI engine operation in the absence of knocking through numerical 1d and 3rd modeling. *Advances in Engineering Software* 95, 38-50.

Bonatesta, F., E. Chiappetta and A. L. Rocca (2014). Part-load particulate matter from a GDI engine and the connection with combustion characteristics. *Applied Energy* 124, 366-376.

Catapano, F., M. Costa, G. Marseglia, P. Sementa, U. Sorge and B. M. Vaglieco (2016b). An experimental and numerical investigation of gdi spray impact over walls at different temperatures. *SAE Technical Paper* 2016(01), 0853.

Catapano, F., P. Sementa and B. M. Vaglieco (2016a). Air-fuel mixing and combustion behavior of gasoline-ethanol blends in a GDI wall-guided turbocharged multi-cylinder optical engine. *Renewable Energy* 96, 319-332.

Cathcart, G. and C. Zavier (2000). Fundamental characteristics of an air-assisted direct injection combustion system as applied to 4-stroke automotive gasoline engines. *SAE Technical Paper* 2000(01), 0256.

Chen, L., Z. Liang, X. Zhang and S. Shuai (2017). Characterizing particulate matter emissions from GDI and PFI vehicles under transient and cold start conditions. *Fuel* 189, 131-140.

Colin, O. and A. Benkenida (2004). The 3-zones extended coherent flame model (ecfm3z) for computing premixed/diffusion combustion. *Oil and Gas Science and Technology - Rev. IFP* 59 (6), 593-609.

Costa, M., F. Catapano, P. Sementa, U. Sorge and B. Vaglieco (2016). Mixture preparation and combustion in a GDI engine under stoichiometric or lean charge: an experimental and numerical study on an optically accessible engine. *Applied Energy* 180, 86-103.

Costa, M., U. Sorge and L. Allocca (2011). Numerical study of the mixture formation process in a four-stroke GDI engine for two-wheel applications. *Simulation Modeling Practice and Theory* 19 (4), 1212-1226.

Costa, M., U. Sorge and L. Allocca (2012). CFD optimization for GDI spray model tuning and enhancement of engine performance. *Advances in Engineering Software* 49, 43-53.

da Costa, R. B. R., C. A. Gomes, R. L. Franco, M. E. Guzzo and F. J. P. Pujatti (2015). E100 stratified lean combustion analysis in a wall-air guided type GDI optical engine. *SAE Technical Paper* 2015(36), 0269.

Dempsey, A. B., B. L. Wang, R. D. Reitz, B. Petersen, D. Sahoo and P. C. Miles (2012). Comparison of quantitative in-cylinder equivalence ratio measurements with CFD predictions for a light duty low temperature

combustion diesel engine. *SAE International Journal of Engines* 5, 162-184.

Drake, M. and D. Haworth (2007). Advanced gasoline engine development using optical diagnostics and numerical modeling. *Proceedings of the Combustion Institute* 31 (1), 99-124.

Esfahanian, V., A. Javaheri, A. Salavati-Zadeh, M. Darzi and M. Mirsoheil (2014). Investigation of natural gas composition effects on knock phenomenon in SI gas engines using detailed chemistry. *Advances in Applied Mechanics and Materials* 493, 239-244.

Ghojel, J. (2010). Review of the development and applications of the wiebe function: A tribute to the contribution of ivan wiebe to engine research. *International Journal of Engine Research* 11 (4), 297-312.

Hallgren, B. E. and J. B. Heywood (2003). Effects of substantial spark retard on SI engine combustion and hydrocarbon emissions. *SAE Technical Paper* 2003(01), 3237.

Iyer, C. O. and J. Yi (2009). Spray pattern optimization for the Duratec 3.5l ecoboost engine. *SAE SAE International Journal of Engines* 2, 1679-1689.

Kaiser, E. W., W. O. Siegl, D. D. Brehob and M. Haghgooie (1999). Engine-out emissions from a direct-injection spark-ignition (DISI) engine. *SAE Technical Paper* 1999-01-1529.

Kuhnke, D. (2004). *Spray wall interaction modeling by dimensionless data analysis*, PhD dissertation. Technische Universitt Darmstadt, Darmstadt, Germany.

Lattimore, T., C. Wang, H. Xu, M. L. Wyszynski and S. Shuai (2016). Investigation of EGR effect on combustion and PM emissions in a DISI engine. *Applied Energy* 161, 256-267.

Marseglia, G., M. Costa, F. Catapano, P. Sementa and B. Vaglieco (2017). Study about the link between injection strategy and knock onset in an optically accessible multi-cylinder GDI engine. *Energy Conversion and Management* 134, 1-19.

Merola, S. S., C. Tornatore and A. Irimescu (2016). Cycle resolved visualization of pre-ignition and abnormal combustion phenomena in a GDI engine. *Energy Conversion and Management* 127, 380-391.

Montanaro, A., L. Allocca, M. Costa and U. Sorge (2016). Assessment of a 3d CFD model for GDI spray impact against wall through experiments based on different optical techniques. *International Journal of Multiphase Flow* 84, 204-216.

Montanaro, A., S. Malaguti and S. Alfuso (2012). Wall impingement process of a multi-hole gdi spray: Experimental and numerical investigation. *SAE Technical Paper* 2012(01), 1266.

Moreira, A. L. N. and M. R. O. Panao (2011). *Handbook of Atomization and Sprays: Theory and Applications*, Springer, New York.

Park, C., S. Kim, H. Kim and Y. Moriyoshi (2012). Stratified lean combustion characteristics of a spray-guided combustion system in a gasoline direct injection engine. *Energy* 41 (1), 401-407.

Rivera, E. A., N. Mastro, J. Zizelman, J. Kirwan and R. Ooyama (2010). Development of injector for the direct injection homogeneous market using design for six sigma. SAE *Technical Paper* 2010(01), 0594.

Schulz, F., J. Schmidt, A. Kufferath and W. Samenfink (2014). Gasoline wall films and spray/wall interaction analyzed by infrared thermography. *SAE SAE International Journal of* 7, 1165-1177.

Semenov, I., P. Utkin, I. Akhmedyanov, P. Pasynkov and A. Popov (2013). Mathematical models and numerical algorithm for the dynamics of gas-droplets flow investigations using high performance computing, in: *Proceeding of International Conference on Parallel and Distributed Computing Systems*, Ukraine.

Sirignano, W. A. (1999). *Fluid dynamics and transport of droplets and sprays*, 2nd Edition, Cambridge University Press, United Kingdom.

Szekely, G. A. and A. C. Alkidas (2005). Combustion characteristics of a spray-guided direct-injection stratified-charge engine with a high-squish piston. *SAE Technical Paper* 2005(01), 1937.

Taskiran, O. O. and M. Ergeneman (2014). Trajectory Based Droplet Collision Model for Spray Modeling. *Fuel* 115, 896-900.

Vanderwege, B. A., Z. Han, C. O. Iyer, R. H. Muoz and J. Yi (2003). Development and analysis of a spray-guided DISI combustion system concept. *SAE Technical Paper* 2003(01), 3105.

Wang, B., S. Mosbach, S. Schmutzhard, S. Shuai, Y. Huang and M. Kraft (2016). Modelling soot formation from wall films in a gasoline direct injection engine using a detailed population balance model. *Applied Energy* 163, 154-166.

Wang, B., Y. Jiang, P. Hutchins, T. Badawy, H. Xu, X. Zhang, A. Rack and P. Tafforeau (2017b). Numerical analysis of deposit effect on nozzle flow and spray characteristics of GDI injectors. *Applied Energy* 204, 1215-1224.

Wang, C., H. Xu, J. M. Herreros, J. Wang and R. Cracknell (2014). Impact of fuel and injection system on particle emissions from a GDI engine. *Applied Energy* 132, 178-191.

Wang, L., J. A. Badra, W. L. Roberts and T. Fang (2017a). Characteristics of spray from a GDI fuel injector for naphtha and surrogate fuels. *Fuel* 190, 113-128.

Wang, X., Y. Ge, L. Liu, Z. Peng, L. Hao, H. Yin, Y. Ding and J. Wang (2015). Evaluation on toxic

reduction and fuel economy of a gasoline direct injection (gdi) powered passenger car fueled with methanol gasoline blends with various substitution ratios. *Applied Energy* 157, 134-143.

Xu, Z., J. Yi, E. W. Curtis and S. Wooldridge (2009). Applications of CFD modeling in GDI engine piston optimization. *SAE SAE International Journal of Engines* 2, 1749-1763.

Yi, J., S. Wooldridge, G. Coulson, J. Hilditch, C. O. Iyer, P. Moilanen, G. Papaioannou, D. Reiche, M. Shelby, B. VanDerWege, C. Weaver, Z. Xu, G. Davis, B. Hinds and A. Schamel (2009). Development and optimization of the ford 3.5l v6 ecoboost combustion system. *SAE SAE*

International Journal of Engines 2, 1388-1407.

Zhao An, Y., Y. qiang Pei, J. Qin, H. Zhao, S. ping Teng, B. Li and X. Li (2016). Development of a PAH (polycyclic aromatic hydrocarbon) formation model for gasoline surrogates and its application for GDI (gasoline direct injection) engine CFD (computational fluid dynamics) simulation. *Energy* 94, 367-379.

Zheng, Z., X. Tian and X. Zhang (2015). Effects of split injection proportion and the second injection time on the mixture formation in a GDI engine under catalyst heating mode using stratified charge strategy. *Applied Thermal Engineering* 84, 237-245.